Electronic Supplementary Material (ESI) for Materials Chemistry Frontiers.

Supporting Information

Magnetic bistable organic ionic plastic crystal with room temperature ion conductivity comparable to NASICON and superionic conduction in a broad temperature window

Yin Qian,*[a] Jin Zhang,[a] Yi-Ming Wang,[a] Wan-Wan Yao,[a] Dong-Sheng Shao,[a] Xiaoming Ren*[a,b,c]

[a] State Key Laboratory of Materials-Oriented Chemical Engineering and College of Chemistry & Molecular Engineering, Nanjing Tech University, Nanjing 211816, P. R. China

[b] College of Materials Science & Engineering, Nanjing Tech University, Nanjing 211816, P. R. China

[c] State Key Laboratory of Coordination Chemistry, Nanjing University 210023, P. R. China

Corresponding authors: Dr. Yin Qian and Prof. Xiao-Ming Ren

Email: yinqian@njtech.edu.cn (YQ); xmren@njtech.edu.cn (XMR)

Contents

Table S6: Dihedral angles (º) between the typical planes (ref. to Figure S5) and Ni…Ni distance (Å) within an anion stack (ref. to Figure S6) at selected temperatures

Figure S7: Rotation angle between two different imidazole rings in **1** at (a) 278 and (b) 388 K.

Figure S8: Variable temperature PXRD patterns in 303–443 K for **1**, indicating the obvious differences between 383 and 398 K as well as between 398 and 408 K, which respectively corresponds to the phase transition from Phase-III to II as well as from Phase-II to I. A new diffraction appears at 2θ~5° in the plastic crystal phase, which is still observed in the cooled phase-III, owing to slow transformation process.

Figure S9: Plots of current against time for **1** acquired at DC voltage of 1V and different temperatures (a) the first measurement at 298 K and cooled down to 298 K from 353 K (b) in 383–408 K (phase-II) on heating (c) in 368–353 K (phase-II) on cooling and (d) in 343–298 K (phase-III) on cooling.

Figure S10: Temperature dependent impedances of **1** (a, b) on heating in 293–453 K and 293–313 K (c) on cooling in 453–293 K.

Figure S11: Experimental and simulated impedance spectra of **1** at 298 K together with the equivalent circuits (where R_i and R_e represent the resistances of ion and electron transport; R_{gb} corresponds to the inter-grain resistance. C_{geom} is a geometrical capacitance owing to a conductor with a finite dielectric permittivity between two parallel metallic electrodes, and such type of parallel plate capacitance acts across the whole configuration, but typically possess very small values. The symbol CPE_{int} denotes the interface capacitance, originated from that the excess ionic charge on one side of the ion-blocking interface is balanced by excess electronic charge in the adjacent metal electrode. CPE_{dif} denotes the capacitance arising from the diffusion of ions), and the impedance spectra are acquired from (a) Gamry Reference 600+ electrochemical workstation and (b) Concept 80 system.

Table S7: Parameters acquired by fit using the circuit elements (R and CPE) at 298 K by Gamry Reference 600+ electrochemical workstation and Concept 80 system

Figure S12: Comparison of impedances of **1** at the same temperatures in the first and the second thermal cycles, showing that the resistance is smaller in the second thermal cycle than in the first one at the same temperature. This is because that the annealed process across a plastic crystal phase make larger amount of lattice defects, which are remained in the crystal phase as the sample was cooled and benefit for the ion transport.

Figure S13: Packing diagrams of **1** at 378 K projected along (a) a-axis (b) c-axis, where the red and green balls represent the centers of two crystallographically different imidazole rings, and are possible cation vacancies in lattice.

Table S8: High ion conducting plastic crystals or their composites

Figure S14: (a) The reproduced plot of magnetic susceptibility versus tempertaure in 1.8–230 K using S = ½ AFM Heisenberg alternating linear spin chain model (b) Plots of $\chi_{m(chain)}T$ vs. T, in which $\chi_{m(chain)}$ values were obtained using spin-gap model in 2–315 K on heating.

References

Experimental section

Reagents and materials

$NiCl_2 \cdot 6H_2O$, iodine and other reagents are of analytical grade and directly used as received from commercial source. 1,3-Diethyl-1H-imidazolium bromide (abbr. [DEIm]Br) and disodium maleonitriledithiolate (abbr. Na_2mnt) were prepared following the procedures published.[1]

Synthesis of [DEIm][Ni(mnt)$_2$] (1)

20 mL H_2O solution with Na_2mnt (0.37 g, 2 mmol) was added to 10 mL H_2O solution containing $NiCl_2 \cdot 6H_2O$ (0.24 g, 1 mmol). The mixture was stirred for 20 min to give a wine-red solution. 10 mL H_2O solution with [DEIm]Br (0.42 g, 2 mmol) was added dropwise to the above wine-red solution, and the dark red microcrystals immediately formed, which were separated by filtration and washed with deionized H_2O (30 mL three times), and then the microcrystals were collected and dried in an oven under vacuum at 60 °C for 2 h. and the dried microcrystals were immersed in 20 mL MeOH solution containing I_2 (0.19 g, 0.75 mmol) and stirred at room temperature for 1 h, the black microcrystals were collected by filtration, washed with MeOH (20 mL four times) up to the filtrate colorless, and then dried under vacuum at room temperature. Yield: ~51 % (the calculation based on the reactant $NiCl_2 \cdot 6H_2O$). Microanalysis for $C_{15}H_{13}N_6NiS_4$ (**1**; %): C, 38.81; H, 2.82; N, 18.10 and found: C, 38.61; H, 2.91; N, 18.19. Selected infrared (IR) spectroscopy bands (cm^{-1}): 3099(w) is attributed to ν_{C-H} in imidazole rings; 2987(s) is assigned to both methyl and methylene; 2209(vs) corresponds to the $\nu_{C\equiv N}$ of the mnt^{2-} ligands; 1567(s) arise from skeleton vibration in imidazole rings; 1160(vs) and 1454(s) are assigned to the ν_{C-S} + ν_{C-C} and $\nu_{C=C}$ of mnt^{2-} ligands. The crystalline sample of **1** was examed by Powder X-ray diffraction (PXRD), and experimental and simulated PXRD patterns are shown in Figure S1.

Physical measurements

Elemental analyses for C, H and N were performed with an Elementar Vario EL III analytic instrument. IR spectrum was recorded on a Nicolet iS5 spectrometer with KBr pellets in 400–4000 cm^{-1}. Room and variable temperature PXRD pattern were

collected using a SHIMADZU XRD-6100 diffractometer with Cu Kα radiation (λ = 1.5418 Å), operated at 40 kV and 40 mA, and the 2θ angle ranges from 5 to 50° with a step of 0.01°. Thermogravimetric analysis (TGA) was carried out by a SDT Q600 thermogravimetric analyzer in 20−800 °C (293−1073 K) under nitrogen atmosphere; The polycrystalline sample was placed in a platinum-pan, the heating rate is 20 °C min^{-1} and the nitrogen flow rate is 100 mL min^{-1}. Differential scanning calorimetry (DSC) was measured on a Pyris 1 power-compensation differential scanning calorimeter with a warming rate of 10 K min^{-1} during the heating-cooling processes. Photographs were recorded with an ECLIPSE LV100 polarizing optical microscope equipped with an LINKAM TH-600PM cool and hot stage.

DC magnetic susceptibility was collected for **1** using Quantum Design MPMS-5 superconducting quantum interference device magnetometer in 1.8−400 K with magnetic field 5000 Oe. Temperature-dependent dielectric and Alternating current (AC) impedance spectra were recorded on a Concept 80 system (Novocontrol, Germany). The powdered disc with a thickness of ~1.23 mm and a diameter of 7.0 mm was prepared using 120 mg of the powdered crystalline sample under a static pressure of 8 MPa for 5 min and sandwiched by platinum electrodes and the AC frequencies span from 1 to 10^7 Hz. The chronoamperometry was recorded by a Gamry Reference 600+ electrochemical workstation. DC resistance was measured by a Digital multimeter (VC890C+), which was checked at room temperature using a Standard 100 Ohm Resistor (used for resistance calibration in Concept 80 system). The powdered sample (260 mg) was filled in a hand-made mould (high temperature resistance Peek plastic, with an inner diameter of 10 mm and external diameter of 20 mm, see below photos), and pressed under a static pressure of 2 MPa for 5 min, and then two platinum foils were attached on two opposite surfaces of sample to connect two hand-made titanium alloy electrodes (see below photos); this sample was used for measurements of both DC resistance and chronoamperometry. The total resistance of both cables and titanium alloy electrodes is 0.8 Ohm at ambient temperature.

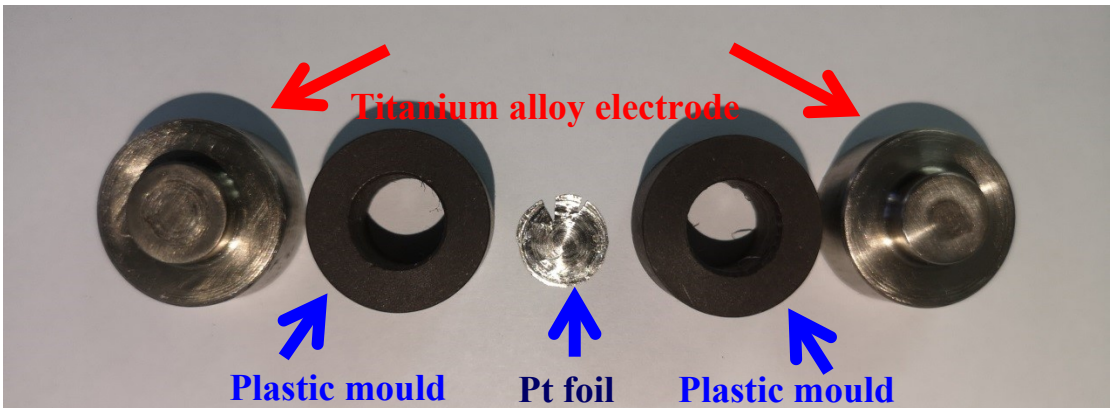

Photos: Hand-made high temperature resistance Peek plastic mould and titanium alloy electrodes for DC resistance and chronoamperometry measurements for **1**.

X-ray Crystallography

Single crystal X-ray diffraction (SCXRD) data were collected for **1** at 298, 368, 378 and 388 K using Graphite monochromated Mo Kα (λ = 0.71073 Å) on a Bruker D8 QUEST Apex III CCD area detector diffractometer. Data reduction and absorption correction were performed with the SAINT[2] and SADABS[3] software packages, respectively. The structures were solved by direct method using the SHELXL-2018[4] software package. The non-hydrogen atoms were anisotropically refined using the full-matrix least-squares method on F^2. All hydrogen atoms were geometrically fixed and placed in ideal position. The crystallographic data and the refinement parameters are listed in Table S1 and S2; the selected bond lengths and angles are summarized in Table S3 and S4, respectively.

Details of crystal structure optimization and total energy calculation of crystal

The geometry optimization of the crystal structure and the calculation of total energy per unit cell were performed for **1** in the framework of density functional theory (DFT) using the CASTEP module.[5,6] The non-modelized crystal structures were taken from X-ray single crystal structure analyses. The generalized gradient approximation (GGA) of Perdew-Burke-Ernzerhof (PBE)[7] potentials have been incorporated for the calculations. The k-points sampling in the Brilliouin zone were set to be 2×1×1 according to the Monkhorst-Pack scheme.[8] The plane wave basis set cut-off at 517 eV and the convergence criterion is 1.0×10^{-5} eV/atom. Other calculating parameters were set to be the default values in the CASTEP code.

Table S1: Crystallographic data and refinement parameters of **1** at 298 and 368 K

Chemical formula	$C_{15}H_{13}N_6NiS_4$	$C_{15}H_{13}N_6NiS_4$
Temp. / K	298	368
CCDC number	2076778	2076779
Formula weight	464.26	464.26
Crystal system	Triclinic	Triclinic
Wavelength/Å	0.71073	0.71073
Space group	*P*−1	*P*−1
a / Å	7.2341(8)	7.2492(6)
b / Å	10.6691(11)	10.7145(10)
c / Å	14.4650(16)	14.8618(13)
α / °	92.838(3)	77.788(3)
β / °	103.236(3)	76.691(2)
γ / °	106.554(3)	74.610(2)
V (Å^3) / Z	1033.82(19) / 2	1069.04(16)/2
ρ / g cm^{-3}	1.491	1.496
F(000)	696	696
θ Ranges	2.91−27.51	1.43–27.56
Index range	−9 ≤ h ≤ 9, −13 ≤ k ≤ 13, −18 ≤ l ≤ 18	-9 ≤ h ≤ 9, -13 ≤ k ≤ 13, -19 ≤ l ≤ 19
Goodness-of-fit on F^2	0.924	1.014
aR1, bwR2 [I>2σ(I)]	0.0532, 0.1479	0.0871, 0.1906
R1, wR2 [all data]	0.0927, 0.1777	0.2160, 0.2542

$^aR_1 = \sum||Fo| - |Fc|/\sum|Fo|$; $^bwR_2 = \{\sum[w(Fo^2 - Fc^2)^2]/\sum[w(Fo^2)^2]\}^{1/2}$

Table S2: Crystallographic data and refinement parameters of **1** at 378 and 388 K

Chemical formula	$C_{15}H_{13}N_6NiS_4$	$C_{15}H_{13}N_6NiS_4$
Temperature/K	378	388 K
CCDC number	2116147	2116214
Formula weight	464.26	464.26
Crystal system	Triclinic	Triclinic
Wavelength/Å	0.71073	0.71073
Space group	*P*−1	*P*−1
a / Å	7.207(6)	7.347(9)
b / Å	10.767(8)	10.848(13)
c / Å	14.526(10)	15.075(18)
α / °	77.77(2)	77.84(4)
β / °	78.81(2)	77.71(5)
γ / °	73.07(3)	74.11(4)
V ($Å^3$) / Z	1043(2)/2	1114(2)/2
ρ / g cm^{-3}	2.250	1.572
F(000)	696	524
θ Ranges	2.66–27.92	2.80–27.58
Index range	$-9 \le h \le 9$, $-13 \le k \le 14$, $-16 \le l \le 18$	$-9 \le h \le 9$, $-14 \le k \le 14$, $-19 \le l \le 19$
Goodness-of-fit on F^2	1.399	2.394
$^aR_1$, $^bwR_2$ [$I>2\sigma(I)$]	0.6112, 0.8922	0.2828, 0.4674
R_1, wR_2 [all data]	0.6361, 0.9057	0.4301, 0.5186

$^aR_1 = \sum||Fo| - |Fc|/\sum|Fo|$; $^bwR_2 = \{\sum[w(Fo^2 - Fc^2)^2]/\sum[w(Fo^2)^2]\}^{1/2}$

Table S3: Selected bond lengths and angles in anion and cation of **1** at 298, 368 K

Bond lengths /Å			
T = 298 K		T = 368 K	
Ni(1)-S(3)	2.1441(17)	Ni(1)-S(1)	2.1371(19)
Ni(1)-S(4)	2.1401(18)	Ni(1)-S(4)	2.1387(18)
Ni(1)-S(2)	2.1443(18)	Ni(1)-S(3)	2.1391(18)
Ni(1)-S(1)	2.1479(18)	Ni(1)-S(2)	2.1480(18)
S(1)-C(1)	1.721(7)	S(1)-C(1)	1.711(7)
S(2)-C(2)	1.716(7)	S(2)-C(2)	1.696(7)
S(3)-C(5)	1.710(7)	S(3)-C(5)	1.685(8)
S(4)-C(6)	1.719(7)	S(4)-C(6)	1.699(8)
N(2)-C(4)	1.136(9)	C(2)-C(1)	1.369(10)
C(6)-C(5)	1.354(10)	C(2)-C(4)	1.431(10)
C(6)-C(8)	1.434(10)	C(1)-C(3)	1.425(10)
C(1)-C(2)	1.355(10)	N(3)-C(7)	1.122(9)
C(1)-C(3)	1.417(10)	C(3)-N(1)	1.147(9)
C(3)-N(1)	1.144(10)	C(6)-C(5)	1.366(10)
C(2)-C(4)	1.436(10)	C(6)-C(8)	1.456(10)
C(5)-C(7)	1.431(10)	N(4)-C(8)	1.146(10)
N(4)-C(8)	1.128(10)	C(5)-C(7)	1.448(10)
C(7)-N(3)	1.127(10)	C(4)-N(2)	1.132(9)
C(9)-N(6)	1.317(10)	N(6)-C(9)	1.292(6)
C(9)-N(5)	1.394(10)	N(6)-C(10)	1.292(6)
N(5)-C(11)	1.326(13)	N(6)-C(14)	1.31(2)
N(5)-C(12)	1.508(14)	C(10)-C(11)	1.292(6)
N(6)-C(10)	1.393(11)	C(11)-N(5)	1.292(6)
N(6)-C(14)	1.418(12)	N(5)-C(9)	1.292(6)
C(10)-C(11)	1.350(15)	N(5)-C(12)	1.46(3)
C(14)-C(15)	1.514(13)	C(14)-C(15)	1.48(3)
C(12)-C(13)	1.483(19)	C(12)-C(13)	1.43(4)
Bond angles/°			
T = 298 K		T = 368 K	
S(3)-Ni(1)-S(4)	92.47(7)	S(1)-Ni(1)-S(4)	178.91(7)
S(3)-Ni(1)-S(2)	178.88(7)	S(1)-Ni(1)-S(3)	87.13(7)
S(4)-Ni(1)-S(2)	86.87(7)	S(4)-Ni(1)-S(3)	92.41(8)
S(3)-Ni(1)-S(1)	87.99(7)	S(1)-Ni(1)-S(2)	92.53(7)
S(4)-Ni(1)-S(1)	178.74(7)	S(4)-Ni(1)-S(2)	87.95(7)
S(2)-Ni(1)-S(1)	92.69(7)	S(3)-Ni(1)-S(2)	178.27(6)
C(1)-S(1)-Ni(1)	103.1(2)	C(2)-S(2)-Ni(1)	103.0(3)
C(2)-S(2)-Ni(1)	102.9(2)	C(1)-S(1)-Ni(1)	103.5(3)
C(5)-S(3)-Ni(1)	103.2(2)	C(6)-S(4)-Ni(1)	102.5(3)
C(6)-S(4)-Ni(1)	103.3(3)	C(5)-S(3)-Ni(1)	103.9(3)
C(5)-C(6)-C(8)	123.4(6)	C(1)-C(2)-C(4)	120.5(7)
C(5)-C(6)-S(4)	120.1(5)	C(1)-C(2)-S(2)	121.2(6)
C(8)-C(6)-S(4)	116.4(6)	C(4)-C(2)-S(2)	118.3(6)
C(2)-C(1)-C(3)	121.8(6)	C(2)-C(1)-C(3)	122.4(7)
C(2)-C(1)-S(1)	120.1(5)	C(2)-C(1)-S(1)	119.7(6)
C(3)-C(1)-S(1)	118.1(6)	C(3)-C(1)-S(1)	117.9(6)

N(1)-C(3)-C(1)	179.6(10)	N(1)-C(3)-C(1)	178.3(9)
C(1)-C(2)-C(4)	121.8(6)	C(5)-C(6)-C(8)	122.5(7)
C(1)-C(2)-S(2)	121.2(5)	C(5)-C(6)-S(4)	121.7(6)
C(4)-C(2)-S(2)	117.1(5)	C(8)-C(6)-S(4)	115.8(7)
N(2)-C(4)-C(2)	179.6(8)	C(6)-C(5)-C(7)	121.7(7)
C(6)-C(5)-C(7)	121.5(6)	C(6)-C(5)-S(3)	119.5(6)
C(6)-C(5)-S(3)	120.9(5)	C(7)-C(5)-S(3)	118.7(7)
C(7)-C(5)-S(3)	117.6(6)	N(3)-C(7)-C(5)	178.9(11)
N(4)-C(8)-C(6)	179.3(9)	N(2)-C(4)-C(2)	179.3(10)
N(3)-C(7)-C(5)	179.4(8)	N(4)-C(8)-C(6)	179.8(9)
N(6)-C(9)-N(5)	103.6(7)	C(9)-N(6)-C(10)	108.0
C(11)-N(5)-C(9)	113.1(9)	C(9)-N(6)-C(14)	138.6(18)
C(11)-N(5)-C(12)	120.5(11)	C(10)-N(6)-C(14)	113.1(18)
C(9)-N(5)-C(12)	126.4(10)	C(11)-C(10)-N(6)	108.0
C(9)-N(6)-C(10)	109.8(8)	N(5)-C(11)-C(10)	108.0
C(9)-N(6)-C(14)	126.9(8)	C(11)-N(5)-C(9)	108.0
C(10)-N(6)-C(14)	123.3(9)	C(11)-N(5)-C(12)	114.8(16)
C(11)-C(10)-N(6)	108.5(9)	C(9)-N(5)-C(12)	135.7(15)
N(6)-C(14)-C(15)	112.7(9)	N(5)-C(9)-N(6)	108.0
C(10)-C(11)-N(5)	104.8(10)	N(6)-C(14)-C(15)	119(2)
C(13)-C(12)-N(5)	115.2(11)	C(13)-C(12)-N(5)	101.8(17)

Table S4: Selected bond lengths and angles in anion and cation of **1** at 378, 388 K

Bond lengths /Å			
T = 378 K		T = 388 K	
Ni(1)-S(1)	2.100(17)	Ni(1)-S(3)	2.152(6)
Ni(1)-S(4)	2.105(17)	Ni(1)-S(2)	2.158(5)
Ni(1)-S(3)	2.118(18)	Ni(1)-S(4)	2.159(6)
Ni(1)-S(2)	2.138(18)	Ni(1)-S(1)	2.168(6)
S(1)-C(1)	1.64(9)	S(1)-C(1)	1.740(18)
S(2)-C(2)	1.69(8)	S(2)-C(2)	1.723(19)
S(3)-C(5)	1.60(8)	S(3)-C(5)	1.72(2)
S(4)-C(6)	1.70(9)	S(4)-C(6)	1.69(2)
N(1)-C(3)	1.06(9)	N(1)-C(3)	1.15(2)
N(2)-C(4)	1.19(13)	N(2)-C(4)	1.12(2)
N(3)-C(7)	1.10(10)	N(3)-C(7)	1.12(3)
N(4)-C(8)	1.02(12)	N(4)-C(8)	1.14(3)
N(7)-C(21)	1.350(11)	C(1)-C(2)	1.37(2)
N(7)-C(17)	1.349(10)	C(1)-C(3)	1.45(3)
N(7)-C(18)	1.400(11)	C(2)-C(4)	1.41(2)
N(8)-C(21)	1.30(2)	C(5)-C(6)	1.35(2)
N(8)-C(16)	1.349(11)	C(5)-C(7)	1.44(3)
N(8)-C(19)	1.400(13)	C(6)-C(8)	1.45(3)
C(16)-C(17)	1.350(12)	N(6)-C(9)	1.29(3)
C(1)-C(2)	1.35(11)	N(6)-C(11)	1.40(3)
C(1)-C(3)	1.46(11)	N(5)-C(9)	1.39(3)
C(2)-C(4)	1.44(14)	N(5)-C(17)	1.42(5)
C(5)-C(6)	1.24(10)	N(5)-C(16)	1.46(4)
C(5)-C(7)	1.44(10)	C(19)-C(22)	1.17(7)
C(6)-C(8)	1.52(13)	C(14)-N(7)	1.41(4)
C(9)-C(10)	1.351(11)	C(14)-C(15)	1.56(4)
C(9)-N(5)	1.349(10)	C(18)-C(17)	1.50(5)
N(5)-C(11)	1.352(11)	C(20)-N(7)	1.33(4)
N(6)-C(10)	1.348(11)	C(20)-N(8)	1.36(5)
N(6)-C(11)	1.349(13)	N(8)-C(10)	1.35(5)
N(6)-C(14)	1.400(11)	C(10)-C(21)	1.51(4)
C(12)-C(13)	1.500(15)	C(11)-C(16)	1.38(4)
C(22)-C(18)	1.500(11)	C(12)-C(13)	1.50(4)
C(14)-C(15)	1.499(14)		
C(19)-C(20)	1.501(11)		
Bond angles/°			
T = 378 K		T = 388 K	
S(1)-Ni(1)-S(4)	178.5(8)	S(3)-Ni(1)-S(2)	178.36(19)
S(1)-Ni(1)-S(3)	86.5(7)	S(3)-Ni(1)-S(4)	91.8(2)
S(4)-Ni(1)-S(3)	92.9(8)	S(2)-Ni(1)-S(4)	88.4(2)
S(1)-Ni(1)-S(2)	93.4(7)	S(3)-Ni(1)-S(1)	87.7(2)
S(4)-Ni(1)-S(2)	87.3(7)	S(2)-Ni(1)-S(1)	92.1(2)
S(3)-Ni(1)-S(2)	178.4(7)	S(4)-Ni(1)-S(1)	179.0(2)
C(1)-S(1)-Ni(1)	102(3)	C(1)-S(1)-Ni(1)	103.3(7)
C(2)-S(2)-Ni(1)	102(3)	C(2)-S(2)-Ni(1)	104.0(7)

C(5)-S(3)-Ni(1)	100(3)	C(5)-S(3)-Ni(1)	102.4(8)
C(6)-S(4)-Ni(1)	100(3)	C(6)-S(4)-Ni(1)	104.2(8)
C(21)-N(7)-C(17)	114(10)	C(2)-C(1)-C(3)	123.3(18)
C(21)-N(8)-C(16)	128(10)	C(2)-C(1)-S(1)	120.1(16)
C(21)-N(8)-C(19)	162(10)	C(3)-C(1)-S(1)	116.5(15)
C(16)-N(8)-C(19)	55(10)	C(1)-C(2)-C(4)	119.2(19)
N(8)-C(16)-C(17)	93(10)	C(1)-C(2)-S(2)	120.4(16)
C(2)-C(1)-C(3)	116(8)	C(4)-C(2)-S(2)	120.3(16)
C(2)-C(1)-S(1)	123(6)	N(1)-C(3)-C(1)	176(3)
C(3)-C(1)-S(1)	120(7)	N(2)-C(4)-C(2)	177(3)
C(1)-C(2)-C(4)	121(9)	C(6)-C(5)-C(7)	125(2)
C(1)-C(2)-S(2)	119(7)	C(6)-C(5)-S(3)	121.8(18)
C(4)-C(2)-S(2)	120(7)	C(7)-C(5)-S(3)	113.3(19)
N(1)-C(3)-C(1)	169(10)	C(5)-C(6)-C(8)	121(2)
N(2)-C(4)-C(2)	162(10)	C(5)-C(6)-S(4)	119.6(18)
C(6)-C(5)-C(7)	118(7)	C(8)-C(6)-S(4)	119.0(18)
C(6)-C(5)-S(3)	126(7)	N(3)-C(7)-C(5)	174(3)
C(7)-C(5)-S(3)	116(7)	N(4)-C(8)-C(6)	179(2)
C(5)-C(6)-C(8)	129(8)	C(9)-N(6)-C(11)	98(3)
C(5)-C(6)-S(4)	121(6)	C(9)-N(5)-C(17)	132(5)
C(8)-C(6)-S(4)	110(7)	C(9)-N(5)-C(16)	99(3)
N(3)-C(7)-C(5)	170(10)	C(17)-N(5)-C(16)	118(5)
N(4)-C(8)-C(6)	170(10)	N(7)-C(14)-C(15)	99(4)
C(10)-C(9)-N(5)	102(10)	N(6)-C(9)-N(7)	81(3)
N(8)-C(9)-N(7)	93(10)	N(7)-C(20)-N(8)	124(5)
C(11)-N(5)-C(9)	105(10)	N(6)-C(9)-N(5)	122(3)
N(7)-C(17)-C(16)	111(10)	C(10)-N(8)-C(20)	95(8)
C(10)-N(6)-C(11)	95(10)	C(21)-N(7)-C(20)	102(4)
C(10)-N(6)-C(14)	130(10)	C(21)-N(7)-C(14)	135(5)
C(11)-N(6)-C(14)	134(10)	C(20)-N(7)-C(14)	123(4)
C(9)-C(10)-N(6)	114(10)	N(8)-C(10)-C(21)	112(8)
N(5)-C(11)-N(6)	111(10)	N(7)-C(11)-N(6)	79(3)
N(6)-C(14)-C(15)	87(10)	C(16)-C(11)-N(6)	116(3)
N(8)-C(19)-C(20)	93(10)	N(7)-C(11)-C(10)	106(6)
		C(16)-C(11)-C(10)	143(6)
		N(6)-C(11)-C(10)	28(4)
		C(11)-C(16)-N(5)	104(4)
		N(5)-C(17)-C(18)	105(6)

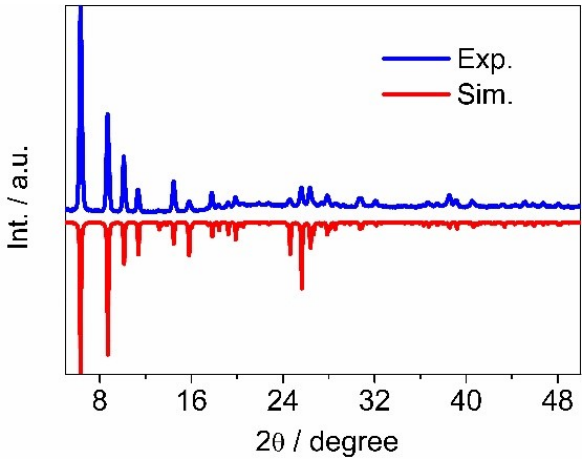

Figure S1: Experimental and simulated PXRD patterns of **1**. The simulated PXRD pattern was obtained from the single crystal X-ray diffraction data at 298 K using Mercury3.1 program.

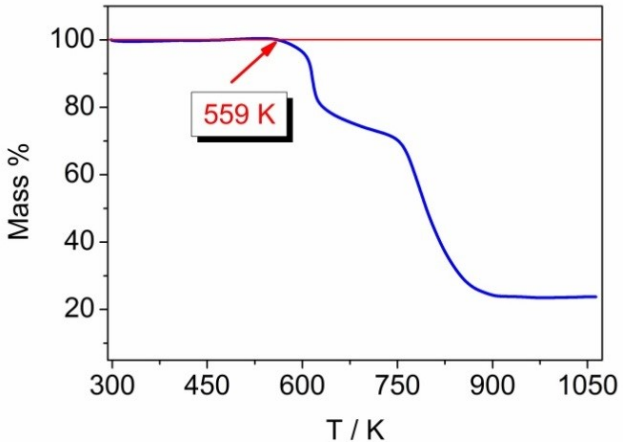

Figure S2: TG plot, indicating that **1** starts thermal decomposition around 559 K.

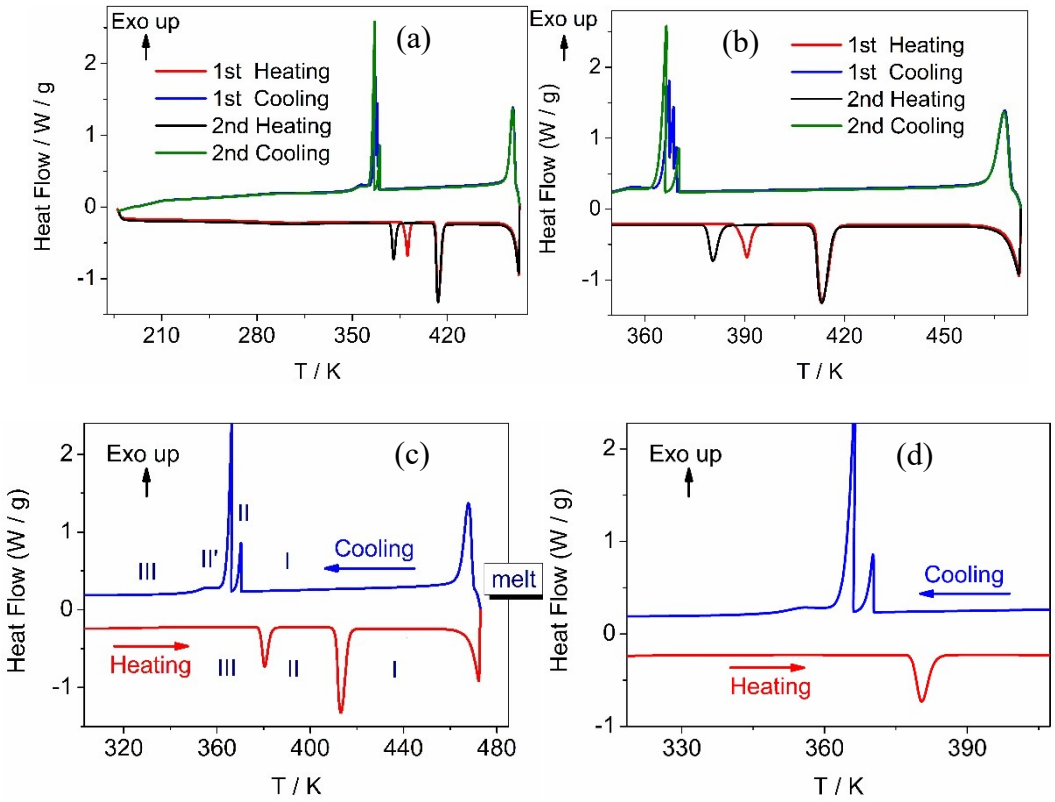

Figure S3: DSC plots of (a, b) two sequential thermal cycles and (c, d) the second thermal cycle for sample-1 in 173–473 K and their larged views around the phase transition.

Table S5: The calculated fusion entropy (ΔS_f) of reported plastic crystals in literature

OIPCs	T_{melt}(K)	ΔS_f(J K^{-1}·mol^{-1})	Ref.
Me_4NDCA	451	13	9
TFSI	338	49	10
$[Zn(HPO_4)(H_2PO_4)_2][ImH_2]_2$	433	7	11
[Gdm-H][NfO]	459	18	12
$[C_2H_4N_3][n\text{-}C_4F_9SO_3]$	463	46	13
$[C_3H_5N_2][CH_3SO_3]$	461	24	14
$[H_2IM][Tf]$	466	19	15
[HMIM][Tf]	385	16	15
[2-MeHIm][TfO]	334	37	16
$[EMIm][Ni(mnt)_2]$	490	26	17
$[DEIm][Ni(mnt)_2]$	465	19	This work

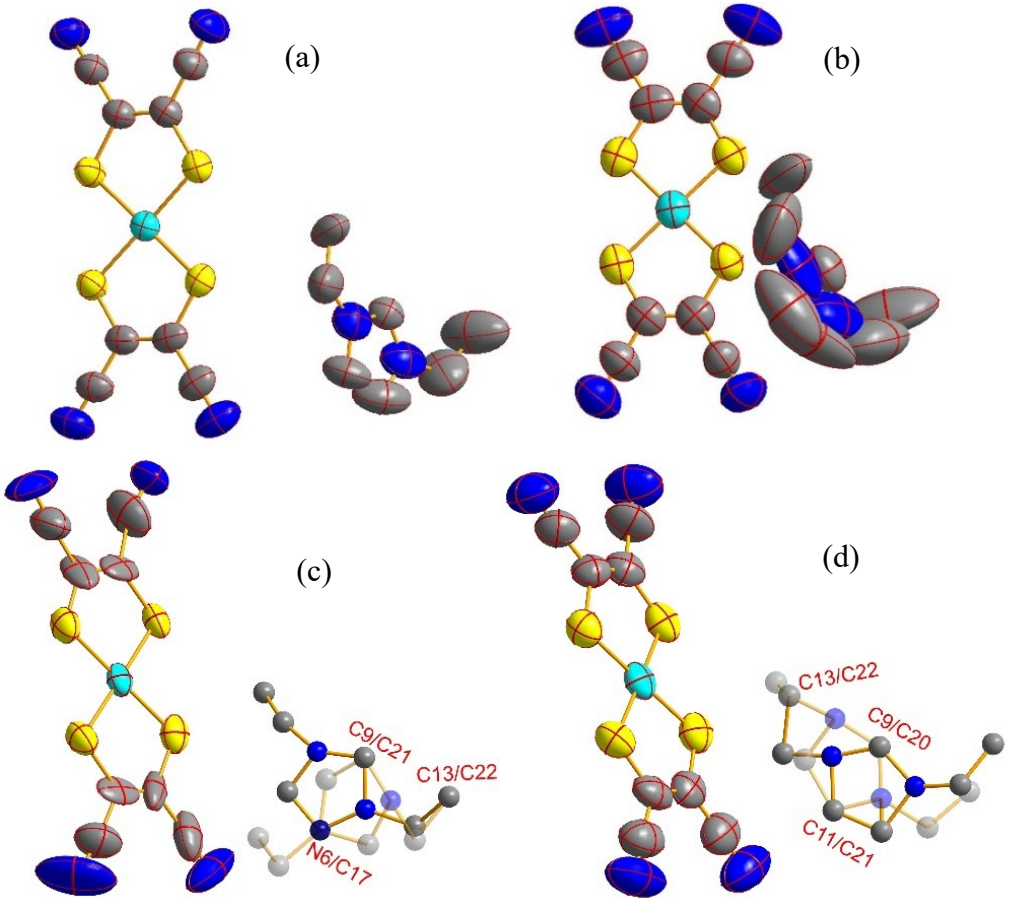

Figure S4: Asymmetric unit of **1** (all displacement ellipsoids of non-hydrogen atoms are drawn at 50% probability level, and hydrogen atoms are omitted for clarity) at (a) 298 K (b) 368 K and (c) 378 K in phase-III (d) 388 K in phase-II.

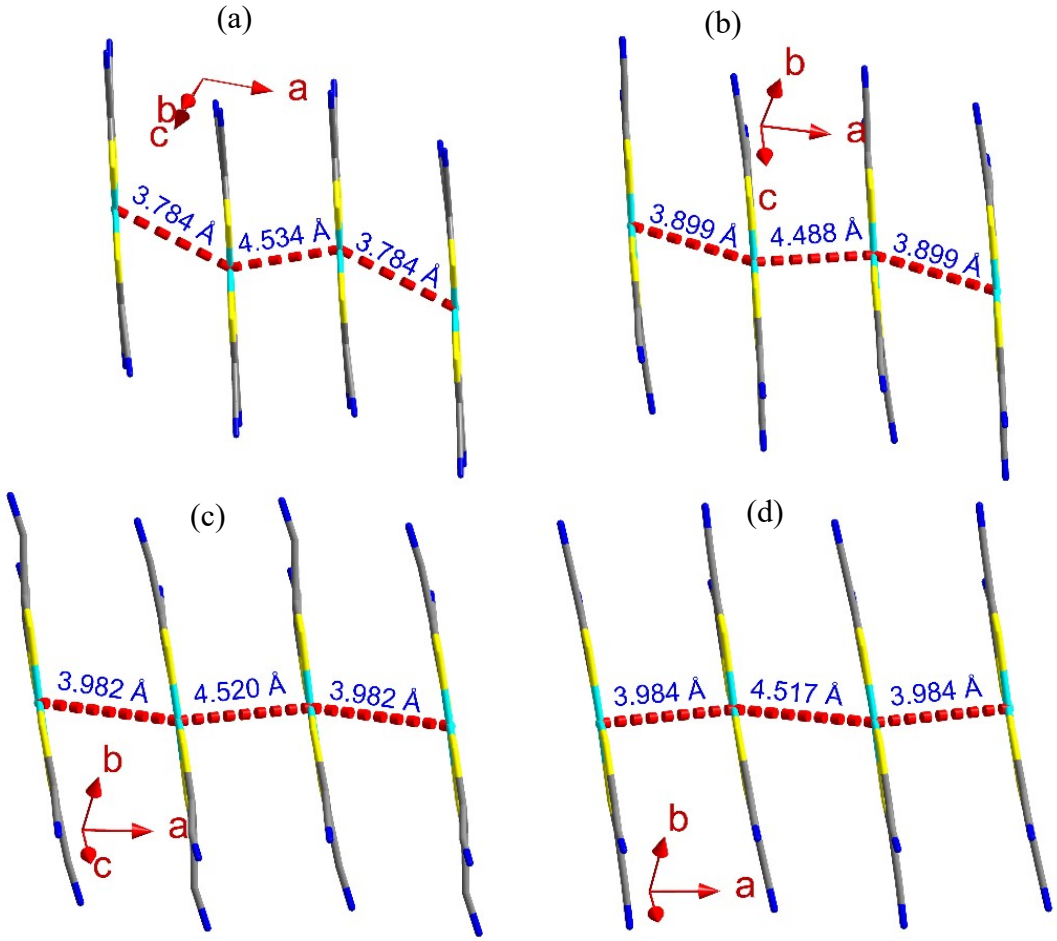

Figure S5: Illustrantion of Ni…Ni distances in the crystal structure of **1** at (a) 298 (b) 368 (c) 378 and (d) 388 K.

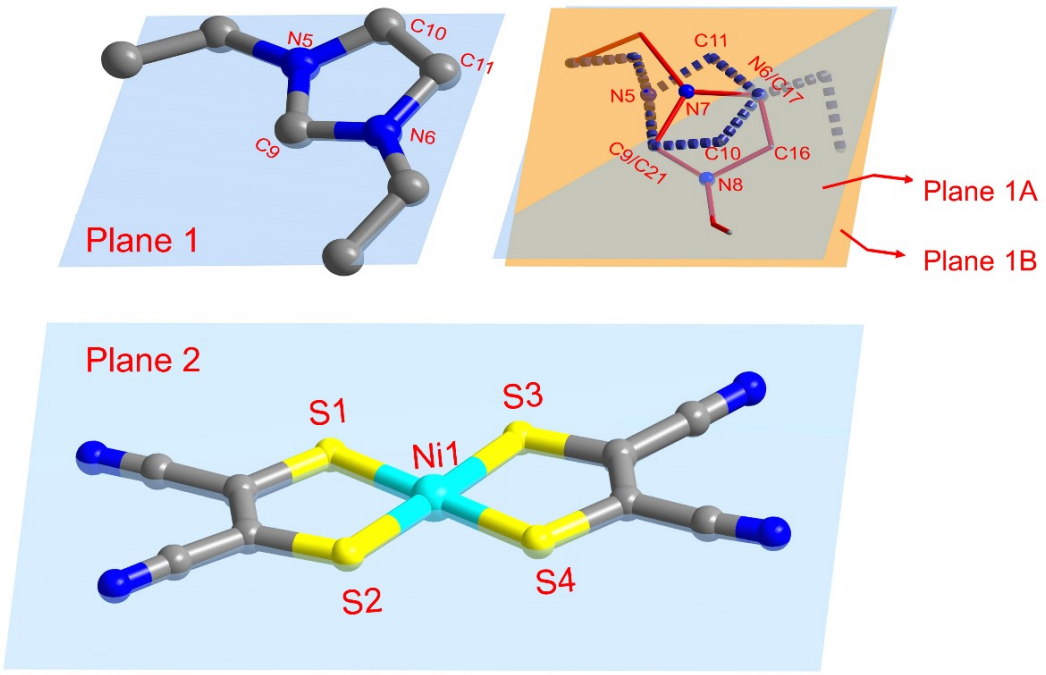

Figure S6: Definition of mean-molecule-plane in Table S6, *i.e.*, plane 1 is the imidazole ring, and plane 1A and 1B represent the planes of different imidazole rings, which contains N5 or N7 atom, respectively; plane 2 is the mean-molecule-plane of anion, defined by Ni1, S1, S2, S3, S4 atoms.

Table S6: Dihedral angles (º) between the typical planes (ref. to Figure S5) and Ni…Ni distance (Å) within an anion stack (ref. to Figure S6) at selected temperatures

Temperature (K)	298	368	378	388
Plane1A-Plane 2	68.9	63.9	65.5	63.3
Plane 1B - Plane 2	–	–	58.6	60.9
Plane 1A- Plane 1B	–	–	8.7	5.4
Ni…Ni distance (Å)	3.767/4.532	3.899/4.488	3.982/4.520	3.984/4.517

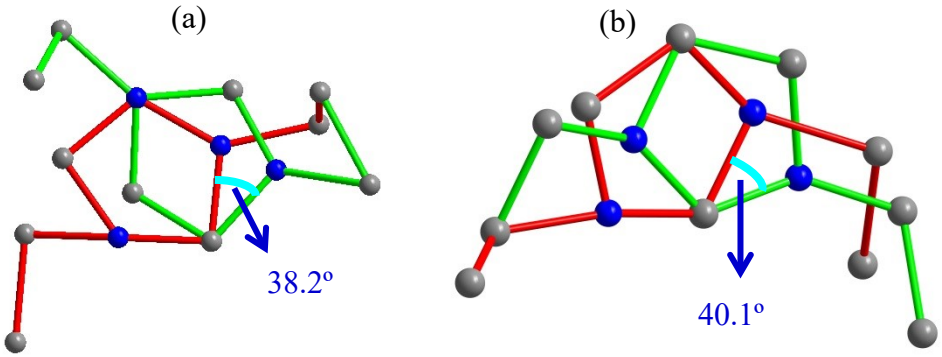

Figure S7: Rotation angle between two different imidazole rings in **1** at (a) 378 and (b) 388 K.

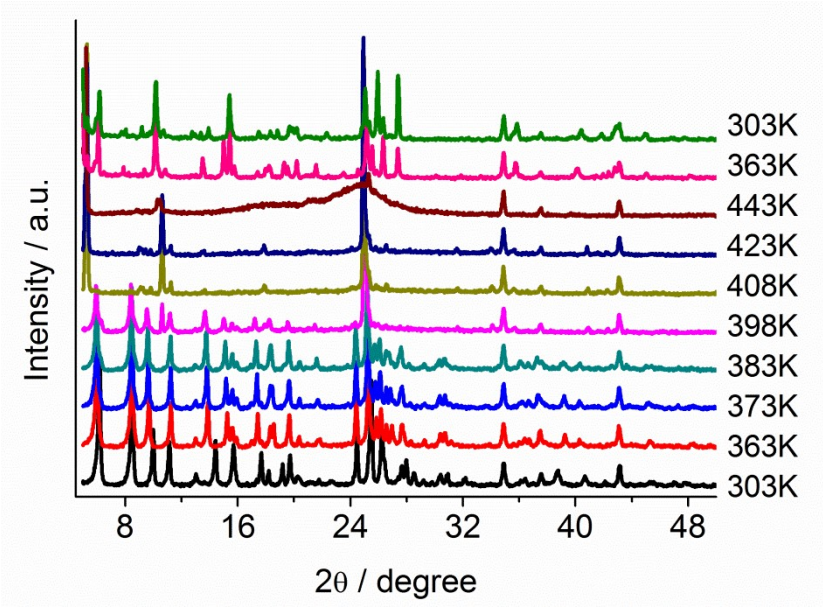

Figure S8: Variable temperature PXRD patterns in 303–443 K for **1**, indicating the obvious differences between 383 and 398 K as well as between 398 and 408 K, which respectively corresponds to the phase transition from Phase-III to II as well as from Phase-II to I. A new diffraction appears at 2θ~5° in the plastic crystal phase, which is still observed in the cooled phase-III, owing to slow transformation process.

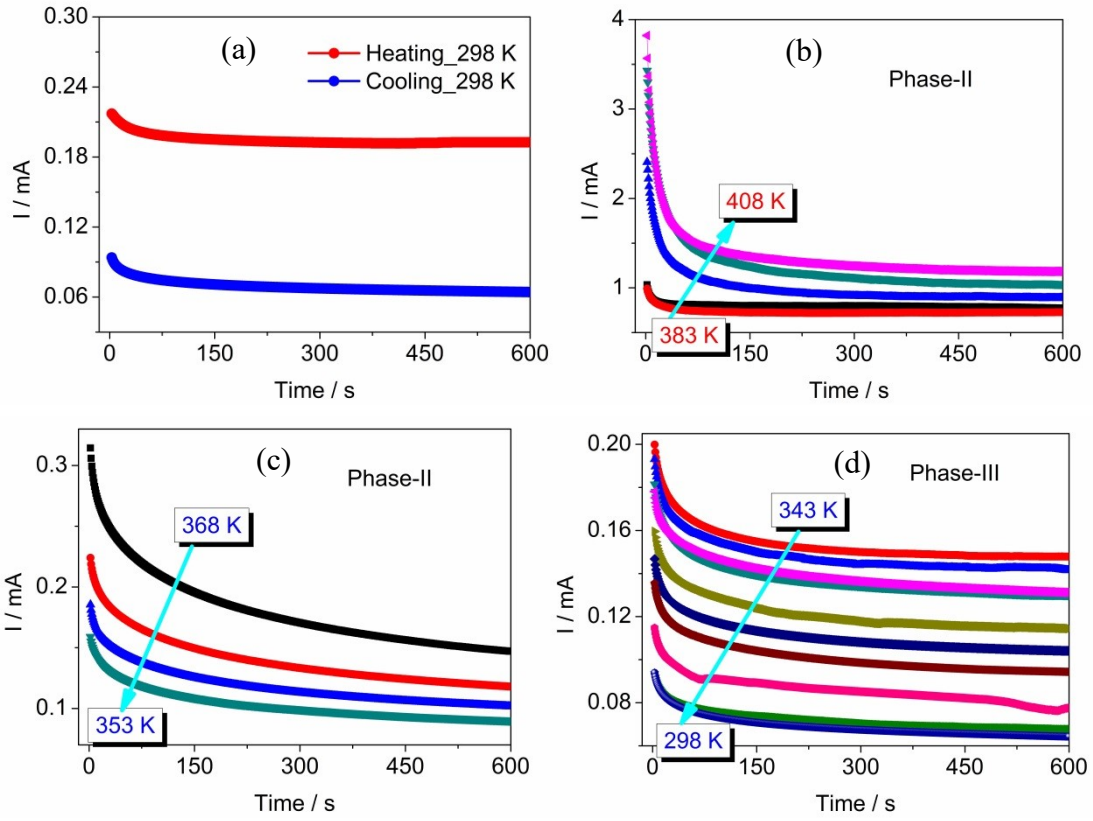

Figure S9: Plots of current against time for **1** acquired at DC voltage of 1V and different temperatures (a) the first measurement at 298 K and cooled down to 298 K from 353 K (b) in 383–408 K (phase-II) on heating (c) in 368–353 K (phase-II) on cooling and (d) in 343–298 K (phase-III) on cooling.

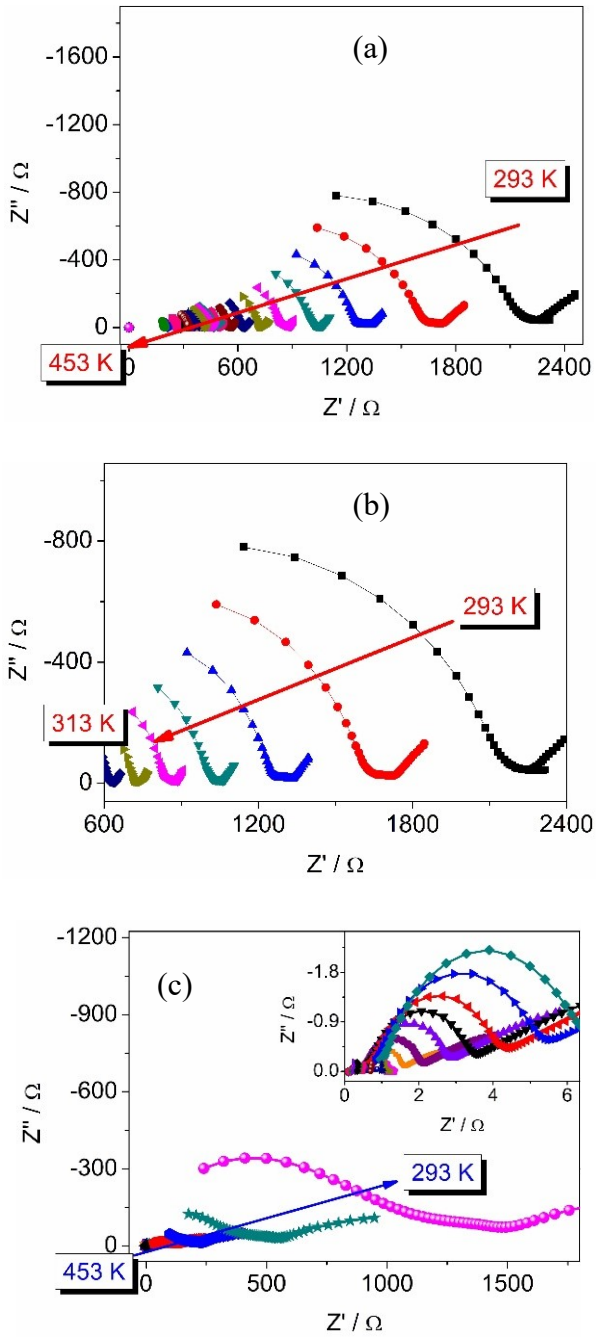

Figure S10: Temperature dependent impedances of **1** (a, b) on heating in 293–453 K and 293–313 K (c) on cooling in 453–293 K.

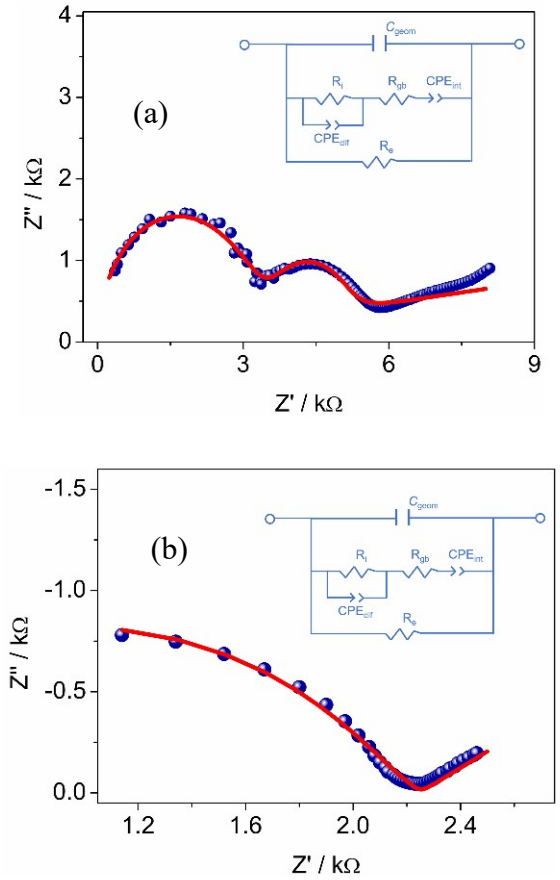

Figure S11: Experimental and simulated impedance spectra of **1** at 298 K together with the equivalent circuits (where R_i and R_e represent the resistances of ion and electron transport; R_{gb} corresponds to the inter-grain resistance. C_{geom} is a geometrical capacitance owing to a conductor with a finite dielectric permittivity between two parallel metallic electrodes, and such type of parallel plate capacitance acts across the whole configuration, but typically possess very small values. The symbol CPE_{int} denotes the interface capacitance, originated from that the excess ionic charge on one side of the ion-blocking interface is balanced by excess electronic charge in the adjacent metal electrode. CPE_{dif} denotes the capacitance arising from the diffusion of ions), and the impedance spectra are acquired from (a) Gamry Reference 600+ electrochemical workstation and (b) Concept 80 system.

Table S7: Parameters acquired by fit using the circuit elements (R and CPE) at 298 K by Gamry Reference 600+ electrochemical workstation and Concept 80 system

	R_i	R_e	R_{gb}	C_{geom}	CPE_{int}-T	CPE_{int}-P	CPE_{dif}-T	CPE_{dif}-T
Gamry	1102	74468	371.2	3.59×10^{-11}	1.16×10^{-4}	0.07	3.78×10^{-9}	1.06
Concept 80	2248	2.71×10^{6}	1.65	4.32×10^{-12}	1.38×10^{-4}	0.44	2.49×10^{-8}	0.51

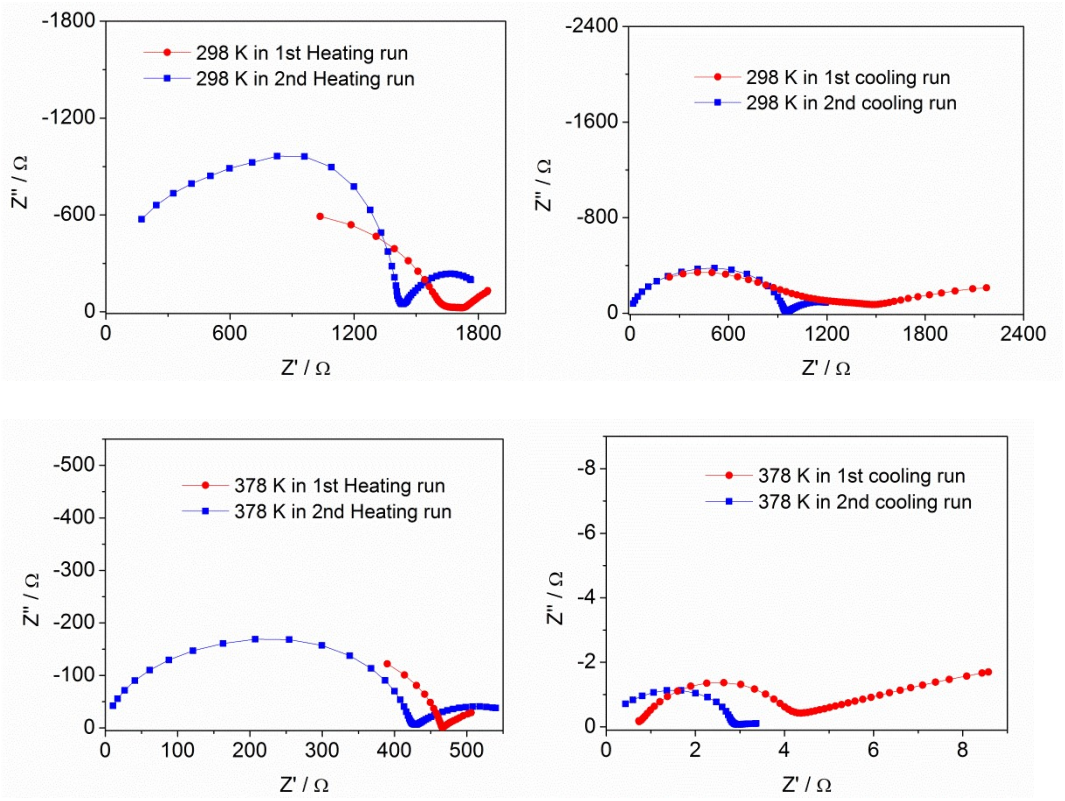

Figure S12: Comparison of impedances of **1** at the same temperatures in the first and the second thermal cycles, showing that the resistance is smaller in the second thermal cycle than in the first one at the same temperature. This is because that the annealed process across a plastic crystal phase make larger amount of lattice defects, which are remained in the crystal phase as the sample was cooled and benefit for the ion transport.

(a)

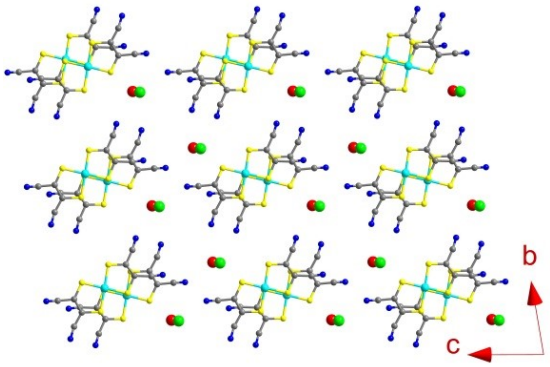

(b)

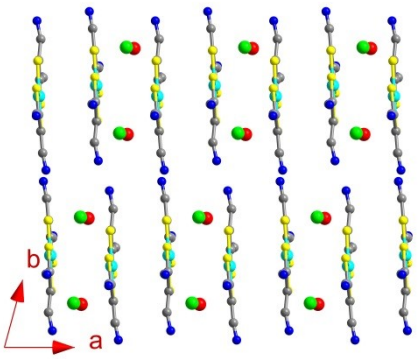

Figure S13: Packing diagrams of **1** at 378 K projected along (a) a-axis (b) c-axis, where the red and green balls represent the centers of two crystallographically different imidazole rings, and are possible cation vacancies in lattice.

Table S8: High ion conducting plastic crystals or their composites

Compound/Composite	σ (S cm^{-1})	Temperature (K)	Ref.
Me_4NDCA	10^{-3}	420	[9]
TFSI	6.2×10^{-3}	333	[10]
$[Zn(HPO_4)(H_2PO_4)_2](ImH_2)_2$	2.6×10^{-4}	403	[11]
[Gdm-H][NfO]	2.1×10^{-3}	458	[12]
$[C_2H_4N_3][n\text{-}C_4F_9SO_3]$	1.1×10^{-4}	453	[13]
$[P_{1,2,2,4}][PF_6]$	1×10^{-3}	393–423	[18]
$[EMIm][Ni(mnt)_2]$	2.1×10^{-1}	453	[17]
$[C_4mpyr][TFSI]$	3×10^{-3}	-	[19]
$PY_{1.1O1}[CF_3BF_3]$	7.7×10^{-3}	-	[19]
$[C_1moxa]$ [DCA]	1.4×10^{-2}	303	[20]
$[C_4mpyr][DCA]$	1.5×10^{-2}	298-343	[21]
$TBA_2[Ni(mnt)_2]$	2.1×10^{-2}	453	[22]
$[C_3H_5N_2]$ $[CH_3SO_3]$	1.0×10^{-2}	458	[23]
PDES/CPE	1.1×10^{-3}	303	[24]
$LiI@P_{1,1}I/COF$	1.4×10^{-2}	423	[25]
$P_{1i444}FSI/NaFSI$	1.0×10^{-4}	303	[26]
$[C_2mpyr][NTf_2]/Na[NTf_2]$	3.0×10^{-4}	333	[27]
KOAc/PVA/Car-30	4.6×10^{-2}	-	[28]
NaOAc/PVA/Car-30	4.5×10^{-2}	-	[28]
$[DEIm][Ni(mnt)_2]$	1.77	453	This work

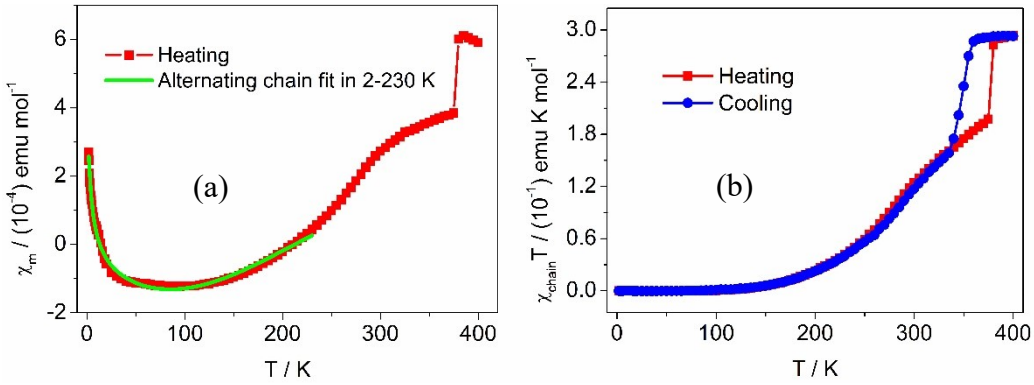

Figure S14: (a) The reproduced plot of magnetic susceptibility versus tempertaure in 1.8–230 K using S = ½ AFM Heisenberg alternating linear spin chain model (b) Plots of $\chi_{m(chain)}T$ vs. T, in which $\chi_{m(chain)}$ values were obtained using spin-gap model in 2–315 K on heating.

The spin Hamiltonian for a Heisenberg alternating linear chain system has the form in Eq. (s1)

$$\hat{H} = -2J\sum_{i=1}^{\frac{n}{2}}[\hat{s}_{2j-1}\hat{s}_{2j} + \alpha\hat{s}_{2j}\hat{s}_{2j+1}] \qquad \text{(s1)}$$

In which J and αJ represent the exchange constant between adjacent spins in the spin chain, respectively, while J < 0 and 0 ≤ α ≤ 1. Based on Eq. (s1), the molar magnetic susceptibility as temperature function, deduced from the cluster approach, is expressed as Eq. (s2)

$$\chi_{chain} = \frac{Ng^2\mu_B^2}{k_BT}\cdot\frac{A + Bx + Cx^2}{1 + Dx + Ex^2 + Fx^3} \qquad \text{(s2)}$$

in Eq. (s2), x=$|J|/k_BT$ and J ≤ 0, and the parameters A-F are constants, which have different values corresponding to the cases of $0 \le \alpha \le 0.4$ and $0.4 \le \alpha \le 1$. The parameters A–F are constants, with different values corresponding to the cases of $0 \le \alpha \le 0.4$ and $0.4 \le \alpha \le 1$.[29] Two different sets of A-F parameters were tried to be fit for the magnetic susceptibility of **1** in 2–230 K, respectively, and the best fit was obtained when α = 0.165(23), J/k_B = –421(5) K, C = 1.92(22)×10^{-3} emu K mol^{-1}, θ = –3.58(51) K and χ_0 = –1.40(2)×10^{-4} emu mol^{-1} (with g = 2.01 fixed, R = 0.992). The

paramagnetic impurity content in **1** is estimated as 0.5% of $S = ½$ molar magnetic susceptibility.

References

1. F. Gu, H. Dong, Y. Li, Z. Sun and F. Yan, Base Stable Pyrrolidinium Cations for Alkaline Anion Exchange Membrane Applications. *Macromolecules* 2014, **47**, 6740−6747.
2. Bruker, *APEX 2*, *SAINT*, *XPREP*, Bruker AXS Inc., Madison, Wisconsin, USA, 2007.
3. Bruker, *SADABS*, Bruker AXS Inc., Madison, Wisconsin, USA, 2001.
4. G. M. Sheldrick, *SHELXS-2014*, Program for the Solution and Refinement of Crystal Structures, University of Göttingen, Göttingen, Germany, 2014.
5. M. D. Segall, P. J. D. Lindan, M. J. Probert, C. J. Pickard, P. J. Hasnip, S. J. Clark and M. C. Payne, First-principles simulation: ideas, illustrations and the CASTEP code, *J. Phys.: Condens. Matter,* 2002, **14**, 2717−2744.
6. V. Milman, B. Winkler, J. A. White, C. J. Pickard, M. C. Payne, E. V. Akhmatskaya and R. H. Nobes, Electronic structure, properties, and phase stability of inorganic crystals: A pseudopotential plane-wave study, *Int. J. Quantum Chem.*, 2000, **77**, 895-910.
7. J. P. Perdew, K. Burke and M. Ernzerhof, Generalized gradient approximation made simple, *Phys. Rev. Lett.*, 1996, **77**, 3865−3868.
8. H. J. Monkhorst and J. D. Pack, Special points for Brillouin-zone integrations, *Phys. Rev. B*, 1976, **13**, 5188-5192.
9. A. J. Seeber, M. Forsyth, C. M. Forsyth, S. A. Forsyth, G. Annat and D. R. MacFarlane, Conductivity, NMR and Crystallographic study of N, N, N, N-tetramethylammonium dicyanamide plastic crystal phases: an archetypal ambient temperature plastic electrolyte material, *Phys. Chem. Chem. Phys.*, 2003, **5**, 2692–2698.
10. Y. Abu-Lebdeh, P. J. Alarco and M. Armand, Conductive Organic Plastic Crystals Based on Pyrazolium Imides, *Angew. Chem. Int. Ed.*, 2003, **42**, 4499–4501.
11. S.Horike, D. Umeyama, M. Inukai, T. Itakura and S. Kitagawa, Coordination Network Based Ionic Plastic Crystal for Anhydrous Proton Conductivity, *J. Am.*

Chem. Soc., 2012, **134**, 7612−7615.

12. X. Chen, H. Tang, T. Putzeys, J. Sniekers, M. Wübbenhorst, K. Binnemans, J. Fransaer, D. E. De Vos, Q. Li and J. Luo, Guanidinium Nonaflate as a Solid-State Proton Conductor, *J. Mater. Chem. A*, 2016, **4**, 12241−12252.
13. J. Luo, A. H. Jensen, N. R. Brooks, J. Sniekers, M. Knipper, D. Aili, Q. Li, B. Vanroy, M. Wübbenhorst, F. Yan, L. V. Meervelt, Z. Shao, J. Fang, Z. H. Luo, D. E. De Vos, K. Binnemans and J. Fransaer, 1, 2, 4-Triazolium Perfluoro-butanesulfonate as An Archetypal Pure Protic Organic Ionic Plastic Crystal Electrolyte for All-Solid-State Fuel Cells, *Energy Environ. Sci.*, 2015, **8**, 1276–1291.
14. J. Luo, O. Conrad and I. F. J. Vankelecom, Imidazolium Methanesulfonate as a High Temperature Proton Conductor, *J. Mater. Chem. A*, 2013, **1**, 2238–2247.
15. H. Zhu, X. Wang, R. Vijayaraghava, Y. Zhou, D. R. MacFarlane and M. Forsyth, Structure and Ion Dynamics in Imidazolium-Based Protic Organic Ionic Plastic Crystals, *J. Phys. Chem. Letti*, 2018, **9**, 3904−3909.
16. A. L. C. Orcid, H. Zhu, K. M. Nairn, M. Forsyth and D. R. MacFarlane, Enhancing Solid-State Conductivity through Acid or Base Doping of Protic Imidazolium and Imidazolinium Triflate Salts. *J. Phys. Chem. C*, 2017, **121**, 27849–27859.
17. Y. Qian, D. S. Shao, W. W. Yao, Z. Y. Yao, L. Wang, W. L. Liu and X. M. Ren, A Promising Phase Change Material with Record High Ionic Conductivity over a Wide Temperature Range of a Plastic Crystal Phase and Magnetic Thermal Memory Effect, *ACS Appl. Mater. Interfaces* 2020, **12**, 28129−28138.
18. L. Jin, K. M. Nairn, C. M. Forsyth, A. J. Seeber, D. R. MacFarlane, P. C. Howlett, M. Forsyth and J. M. Pringle, Structure and Transport Properties of a Plastic Crystal Ion Conductor: Diethyl(methyl)(isobutyl)phosphonium Hexafluoro-phosphate, *J. Am. Chem. Soc.*, 2012, **134**, 9688–9697.
19. Z. B. Zhou, H. Matsumoto and K. Tatsumi, Cyclic Quaternary Ammonium Ionic Liquids with Perfluoroalkyltrifluoroborates: Synthesis, Characterization, and Properties, *Chem. Eur. J.*, 2006, **12**, 2196–2212.

20. T. J. Simons, P. M. Bayley, Z. Zhang, P. C.; Howlett, D. R. MacFarlane, L. A. Madsen and M. Forsyth, Influence of Zn^{2+} and Water on the Transport Properties of a Pyrrolidinium Dicyanamide Ionic Liquid, *J. Phys. Chem. B*, 2014, **118**, 4895−4905.
21. C. S. M. Kang, R. Yunis, H. Zhu, C. M. Doherty, O. E. Hutt and J. M. Pringle, Ionic Liquids and Plastic Crystals Utilizing the Oxazolidinium Cation: the Effect of ether Functionality in the Ring. *Mater. Chem. Front.*, 2021, **5**, 6014–6026.
22. Y. Qian, D. S. Shao, W. W. Yao, N. Wan, X. Z. Wang and X. M. Ren, Ion Conduction and Complicated Phase Transition Behaviors in an Organic Ion Plastic Crystal, [Tetra-n-butylammonium]$_2$[Ni(maleonitriledithiolate)$_2$], *J. Phys. Chem. C*, 2020, **124,** 20722−20729.
23. J. Luo, O. Conrad and I. F. J. Vankelecom, Imidazolium Methanesulfonate as a High Temperature Proton Conductor, *J. Mater. Chem. A*, 2013, **1**, 2238–2247.
24. C. Wang, H. Zhang, S. Dong, Z. Hu, R. Hu, Z. Guo, T. Wang, G. Cui and L. Chen, High Polymerization Conversion and Stable High-Voltage Chemistry Underpinning an In Situ Formed Solid Electrolyte, *Chem. Mater.*, 2020, **32**, 9167−9175.
25. Z. Wu, Q. Xu, J. Li and X. M. Zhang, Liquid-Like Phase of N, N-Dimethylpyrrolidinium Iodide Impregnated into COFs Endows Fast Lithium Ion Conduction in the Solid State, *Chem. Eur. J.*, 2021, **27**, 4583–4587.
26. F. Makhlooghiazad, J. Guazzagaloppa, L. A. O'Dell, R. Yunis, A. Basile, P. C. Howlett and M. Forsyth, The Influence of the Size and Symmetry of Cations and Anions on the Physicochemical Behavior of Organic Ionic Plastic Crystal Electrolytes Mixed with Sodium Salts, *Phys. Chem. Chem. Phys.*, 2018, **20**, 4721–4731
27. M. Forsyth, T. Chimdi, A. Seeber, D. Gunzelmann and P. C. Howlett, Structure and Dynamics in an Organic Ionic Plastic Crystal, N-ethyl-N-methyl Pyrrolidinium Bis(trifluoromethanesulfonyl)amide, Mixed with a Sodium Salt, *J. Mater. Chem. A*, 2014, **2**, 3993–4003
28. T. Ye, Y. Zou, W. Xu, T. Zhan, J. Sun, Y. Xia, X. Zhang and D. Yang, Poorly-

Crystallized Poly (vinyl alcohol)/Carrageenan Matrix: Highly Ionic Conductive and Flame-retardant Gel Polymer Electrolytes for Safe and Flexible Solid-State Supercapacitors, *J. Power Sources*, 2020, **475,** 228688.

29. J. C. Bonner and Fisher, M. E. Linear Magnetic Chains with Anisotropic Coupling. *Phys. Rev.* 1964, **135**, A640−A658.